

Journal of Biomedical Optics

SPIEDigitalLibrary.org/jbo

Thermographic investigation of tumor size, and its correlation to tumor relative temperature, in mice with transplantable solid breast carcinoma

Michal Tepper
Asaf Shoval
Oshrit Hoffer
Hila Confino
Michael Schmidt
Itzhak Kelson
Yona Keisari
Israel Gannot

Thermographic investigation of tumor size, and its correlation to tumor relative temperature, in mice with transplantable solid breast carcinoma

Michal Tepper,^{a*} Asaf Shoval,^{a*} Oshrit Hoffer,^{a*} Hila Confino,^b Michael Schmidt,^c Itzhak Kelson,^c Yona Keisari,^b and Israel Gannot^a

^aTel Aviv University, Department of Biomedical Engineering, Faculty of Engineering, Tel Aviv 6997801, Israel

^bTel Aviv University, Department of Clinical Microbiology and Immunology, Sackler Faculty of Medicine, Tel Aviv 6997801, Israel

^cTel Aviv University, School of Physics and Astronomy, Raymond and Beverly Sackler Faculty of Exact Sciences, Tel Aviv 6997801, Israel

Abstract. Treating cancer is one of the major challenges of modern medicine. Since mice models are an important tool in cancer treatment research, it is required to assess murine tumor development. Existing methods for investigating tumor development are either high cost and limited by their availability or suffer from low accuracy and reproducibility. In order to overcome these drawbacks, thermography may be used. DA3 breast cancer carcinoma tumors in 12 Balb/c mice were thermally imaged and monitored for a period of several weeks. Eight mice were treated with diffusing alpha emitters radiation therapy (DaRT) wires, while four were treated with inert wires. For large tumors, the area was estimated by analyzing thermal images and was found to be in correlation with manual caliper measurements. In addition, the correlation between tumor area and relative temperatures was calculated and compared to previous works. Temperature differences were larger for tumors treated with DaRT wires than tumors with inert wires. These correlations can be used to assist in tumor size estimation and reveal information regarding its metabolic state. Overall, thermography was shown to be a promising tool for assessing tumor development with the additional advantages of being nonradiative and potentially providing indication of intratumoral biological processes. © 2013 Society of Photo-Optical Instrumentation Engineers (SPIE) [DOI: 10.1117/1.JBO.18.11.111410]

Keywords: thermography; biomedical optics; biophotonics; medical imaging; thermal imaging; infrared imaging.

Paper 130244SSR received Apr. 15, 2013; revised manuscript received Jun. 23, 2013; accepted for publication Jul. 10, 2013; published online Aug. 12, 2013.

1 Introduction

Treating cancer is one of the major challenges of modern medicine. A large number of methods are utilized, such as surgery, chemotherapy, and radiation therapy. Since mice models are an important tool in cancer treatment research, there is a necessity to assess tumor development in mice. One method to assess tumor development is to image the tumor by one of several modalities [e.g., computed tomography (CT), magnetic resonance imaging (MRI), and positron emission tomography (PET)] by which size and location of the tumor can be measured.¹ Yet, these modalities are limited by their availability and cost. Mechanical calipers are commonly used for tumor size assessment. However, this method suffers from low accuracy and reproducibility.^{2,3}

Thermography, based on the detection of mid-IR radiation inertly emitted from the surface of a measured object, is an imaging modality that enables accurate, high-resolution surface temperature measurements.⁴ This method is highly suitable for overcoming the drawbacks described, due to its rapid, non-ionizing, noninvasive, and low-cost nature. Thermal imaging has been investigated thoroughly and utilized for numerous medical applications: peripheral vascular disorders,^{5–7} inflammatory diseases,⁸ and cancer detection, especially breast

cancer.^{9–16} The high sensitivity of this method to changes on the surface is extremely valuable in cancer detection, as the majority of human cancers arise from epithelial cells. Since malignant tumors are characterized by abnormal metabolic and perfusion rates,^{17–19} they are expected to show abnormal temperature distribution compared to their healthy surroundings.^{9,20} This characteristic can be used to detect the tumor and evaluate its properties,^{21,22} although improving the accuracy of automated algorithms *in vivo* is a great challenge.

Transplantable tumors in mice exhibit an interesting characteristic: the surface temperature of the tumor is lower than the temperature of the healthy skin tissue surrounding it.^{23–25} This temperature difference was measured before in parallel to the changes in tumor size.^{23,24} However, the correlation between these factors over time was never investigated and calculated as well as its dependence on the tumor's condition.

This paper presents an investigation of the correlation between tumor-healthy tissue temperature differences and tumor area in DA3 breast cancer carcinoma tumors. This correlation was also compared to data extracted from previously published experiments by other groups.^{23,24} The ability to estimate tumor sizes by analyzing the thermal images was investigated and compared to the conventional method of caliper measurements. In addition, the dependence of the spatial temperature differences on changes in tumor's area and treatment was investigated as well.

*These authors contributed equally to this work.

Address all correspondence to: Michal Tepper, Tel Aviv University, Department of Biomedical Engineering, Faculty of Engineering, Tel Aviv 6997801, Israel. Tel: (972)36406592; Fax: (972)36407939; E-mail: michalt5@post.tau.ac.il

2 Methods and Materials

Female Balb/c 10.5-weeks-old mice were each injected with 5×10^5 DA3 murine breast carcinoma cells (in a 150 μL phosphate-buffered saline solution) below their mammary glands. Mice were handled in familiar conditions by expert animal license holders and thermal images were taken while the mice were awake and without any sedation. The surroundings of each tumor were shaved prior to the measurements, as much as tumor state allowed.

In the first experiment, three mice were thermally imaged at nine different occasions during the period between 13 and 46 days (days 13, 14, 18, 27, 33, 36, 39, 42, and 46 of the experiment) after tumor injection (mouse #3 was imaged only eight times, starting from day 14). Treatment was initiated 33 days after tumor cells were injected.

In the second experiment, nine mice with single main tumors were thermally imaged at four different occasions during the period between 15 and 29 days (days 15, 18, 22, and 29 of the experiment) after the tumor injection. Treatment was initiated at day 15, 14 days after tumor cells were injected. Two mice died during the experiment and participated only in the first two imaging days.

The thermal images were captured using a ThermoVision A40 (FLIR©) thermal camera. This camera can detect thermal differences as low as 0.08°C , with a spatial resolution of 1.3 mrad, and produces thermal images of 240×320 pixels. The thermal camera was placed 30 cm from the mouse to capture and record its temperature during the experiments. IR images captured during the experiments were transferred to the PC by a FireWire connection. The data from the thermal images obtained by the camera were analyzed using the thermal camera software (ThermaCAM Researcher Professional, FLIR) and Matlab. Images in the visible spectrum were taken by a Panasonic© DMC-ZS10 Lumix camera (14 megapixels) for the first experiment and by a Samsung© I9300 Galaxy S3 (8 megapixels and autofocus) for the second experiment.

Size was calibrated by including a ruler with a known width in each image. The number of pixels required to image the ruler was measured and the ratio of mm/pixel for each image was calculated and used to estimate the size of imaged objects by multiplying it by their size in pixels.

The grown tumors are approximately elliptical. Manual measurements of the widths (w), lengths (l), and depths (d) of these tumors were taken by a caliper (without applying compression) following each imaging session. Tumor area and volume approximations were calculated using ellipsoid area and volume formulas:²

$$A = \frac{\pi}{4}(w \cdot l), \quad (1)$$

$$V = \frac{\pi}{6}(w \cdot l \cdot d). \quad (2)$$

Tumor depth measurements were found to be highly unstable due to the difficult measurement in this dimension. The relatively small depth of the tumors (around 3 mm) led to large errors in volume calculations. Therefore, it was decided to neglect the depth dimension and use only area estimations in order to improve the estimation's accuracy.

The mice were treated with diffused alpha radiation therapy (DaRT)²⁶⁻²⁸ wires. In this method, tumors are treated by the insertion of specially prepared radioactive sources, impregnated with small activities of a parent alpha emitting isotope (^{224}Ra), which continually releases its short-lived alpha emitting daughter atoms from the source surface. These atoms can then spread within the tumor by the combined effects of diffusion and convection (vascular and possibly interstitial), forming a region of tumor cell destruction, where a lethal dose is delivered through their alpha decays.²⁹ Treated mice were injected intratumoral with an 11-mm-long DaRT wire (10 mm of which are active).

In the first experiment, mouse #1 and mouse #2 were injected with 60 kBq wires. Mouse #3 was injected with an inert wire as a control. In the second experiment, mice #1 to #6 were injected with 40 kBq wires. Out of those, two mice (#2 and #3) received 25 mg/kg cyclosporine per day in addition to DaRT treatment. This was done in order to inhibit their immune system and was expected to affect metastasis formation only (and not the tumor itself). Mouse #1 received glucose solution in addition to DaRT treatment. Mice #7 to #9 were injected with inert wires.

3 Results

Initially, thermal images of three mice were analyzed in order to evaluate the ability to estimate tumor areas and to observe changes in the temperature of tumors and their surroundings. In this initial experiment, thermal images of the three mice were obtained and analyzed to create an optimal basis for comparison in order to better observe the tumor and the undergoing processes. First, the tumor was identified by visual examination of the image. Next, using the size calibration ratio for each image, a 2 cm \times 2 cm-equivalent section of the image was cropped out of the main image. The cropped section included the tumor in its center and the healthy tissue surrounding it (tumor diameter was always smaller than this length). Images were rotated if necessary in order to show the tumor in approximately the same orientation.

An example of a cropped tumor image can be seen in Fig. 1. The figure demonstrates some of the difficulties arising in the

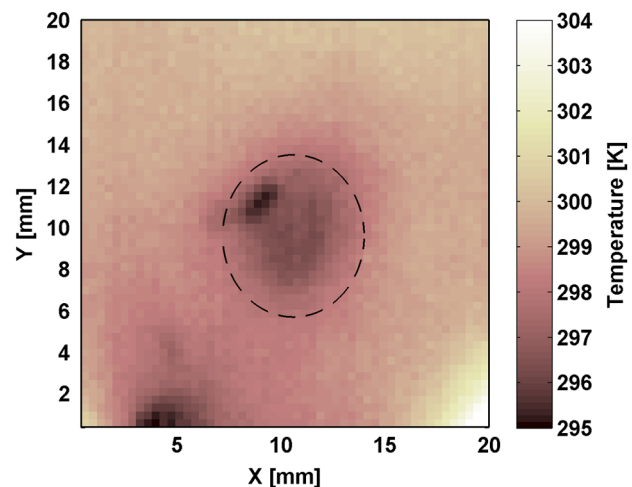


Fig. 1 2 \times 2 cm thermal image of tumor surroundings for mouse #3, day 21. The colder region in the center of the image is the tumor. The inserted inert wire can be seen as a relatively cold line, adjacent to the upper left side of the tumor. Other tissues and features appear on the bottom of the image. The estimated tumor area is marked by the elliptical black dashed line.

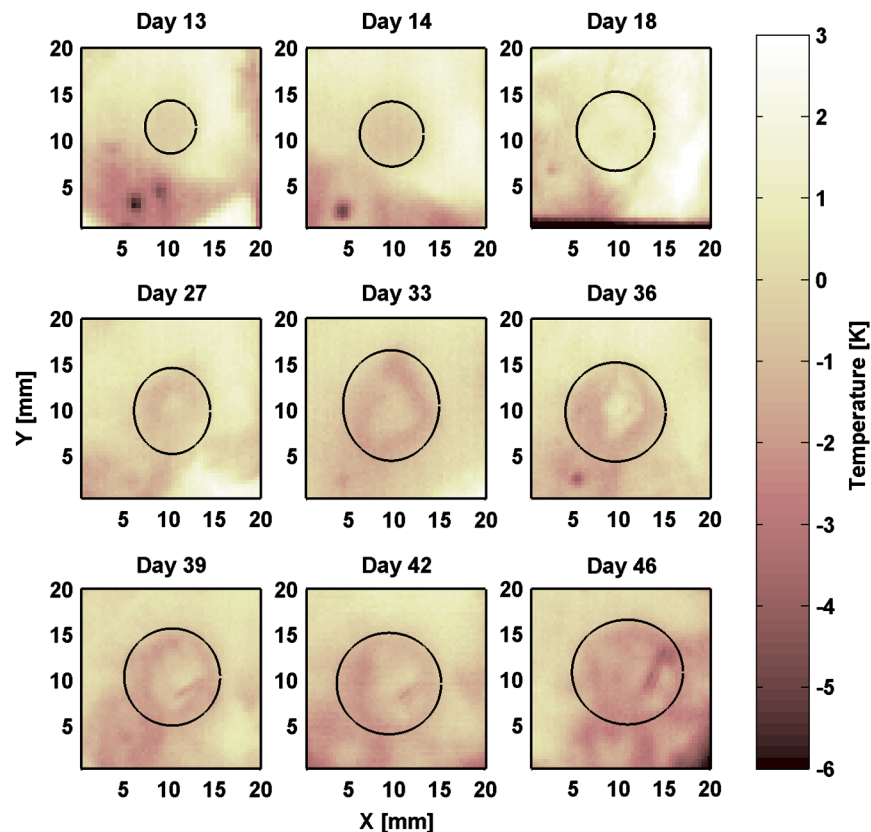


Fig. 2 Thermal images of tumor area for mouse #1. Estimated tumor boundaries are marked by a black ellipse.

analysis of the images. Although the tumor can be easily identified, its borders cannot be conclusively determined. Other features, irrelevant for the analysis, can be seen in the lower part of the image, such as the background and nearby tissues.

Another feature of interest in this figure is the treatment wire (inert, in this case), which can be seen as a colder line adjacent to the upper left side of the tumor.

An automated algorithm was developed to detect the tumor and its boundaries but produced poor results due to the described characteristics. Therefore, for each image the tumor and its boundaries were identified manually and were represented by an elliptical shape. The estimated boundaries of the tumor in Fig. 1 were marked with a dashed black line.

When observing thermal images of the same mouse on different days, the healthy skin tissue temperature varies due to environmental conditions and the mouse's physical state. In order to show thermal changes in the tumor, the temperature scales of all the images were standardized by reducing the healthy tissue temperature for each day. The healthy tissue temperature was determined by examining the image and manually selecting an adjacent tissue with representing temperature (that can be seen on most of the tissues around the tumor). This temperature was estimated from a shaved region in the abdomen area representing a healthy skin tissue.

Figures 2 to 4 show the processed thermal images obtained for mice #1 to #3, respectively. To allow for easier comparison between images, the same temperature scale was used for all images.

Transplantable DA3 tumors are characterized by the development of a necrotic region in the center of the tumor due to a poor blood flow there. In this experiment, the skin above the necrotic

area (the necrotic shell) of mouse #1 has broken down between days 18 and 27, exposing the tissues beneath it and forming a cavity. The thermal images clearly show the colder boundary region of this wound (which is also a part of the tumor). This behavior was not seen in mice #2 and #3, which showed convex tumor morphology.

This breakdown of the necrotic shell in mouse #1 exposed the internal underlying processes occurring in the tumor and allowed *in vivo* examination of the effects caused by the DaRT treatment. Specifically, the thermal image of day 46 reveals small (2 mm diameter), round, hotter regions in the tumor, which may show the biological response to the DaRT wire treatment.

The estimated area of the tumors on each day was calculated according to the area of the representing ellipse. The estimated area was compared with the caliper-measured area. The comparison is shown in Fig. 5. The figure shows a relatively good qualitative fit as the slope of both graphs is similar for each mouse.

Tumor morphology seems to have an effect on the way tumor area is estimated according to the thermal image, leading to a constant offset in tumor area estimation. For mouse #1, which showed concave tumor morphology, the estimation was slightly but consistently above the manual measurement. On the other hand, for mice #2 and #3, which showed convex tumor morphology, the estimation was slightly but consistently below the manual measurement. As presented in Fig. 6, this deviation might be explained in the following way: For the concave morphology of mouse #1 tumor, tumor edges are more exposed to air compared to convex morphology. Therefore, the cooler area extends, resulting in the determination of a larger tumor

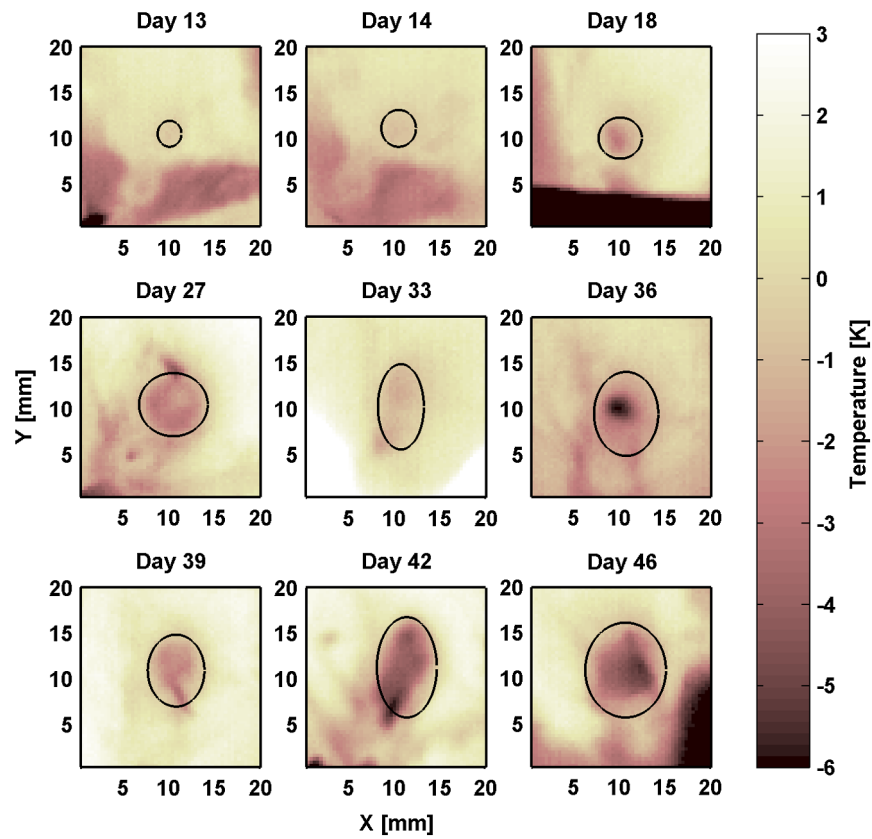


Fig. 3 Thermal images of tumor area for mouse #2. Estimated tumor boundaries are marked by a black ellipse.

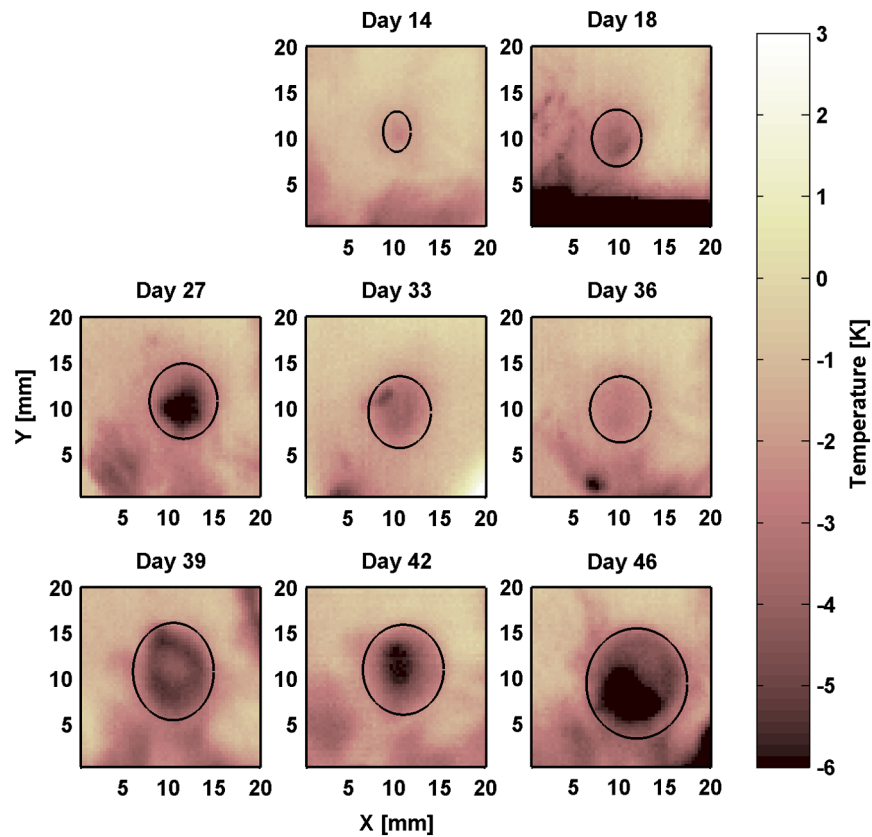


Fig. 4 Thermal images of tumor area for mouse #3. Estimated tumor boundaries are marked by a black ellipse.

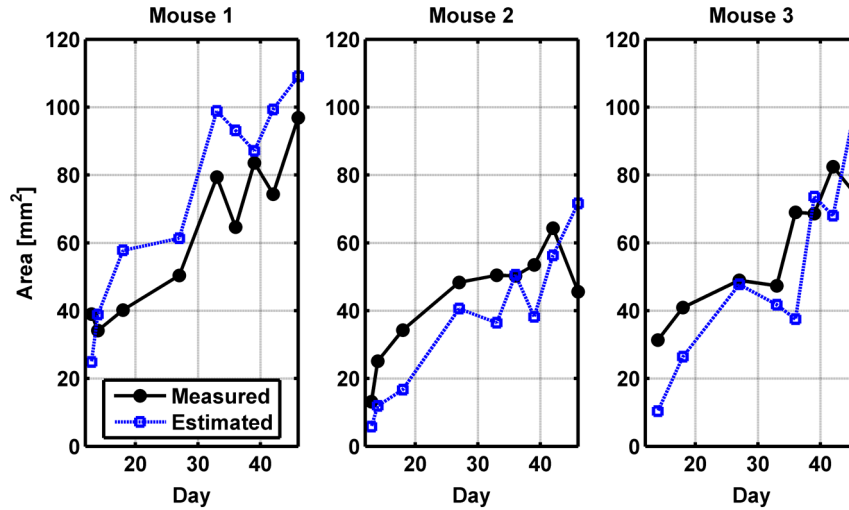


Fig. 5 Caliper measurements of the tumor's area (circular markers) and estimation from the thermal images (square markers).

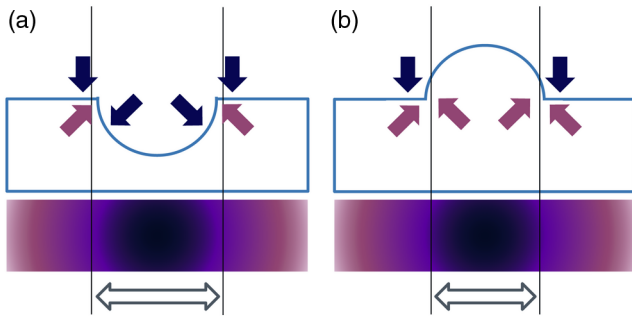


Fig. 6 (a) concave tumor morphology causes an overestimation of tumor area due to cooling of tumor edges. (b) convex tumor morphology causes an underestimation of tumor area due to heating of tumor edges.

area. In mice #2 and #3, the convex tumor shape creates a larger distance between the air and the healthy surrounding tissues, thus allowing the healthy tissues to slightly heat the tumor boundaries, leading to underestimation of the tumor's area.

The temperature profile inside the estimated tumor boundaries was extracted and used to calculate the average and minimal tumor temperatures. These temperatures, along with the temperature of the healthy skin tissue, were used to calculate the average and maximal temperature differences between the tumor and the healthy skin, shown in Figs. 7 and 8, respectively.

As the figures show, the average and maximal temperature differences are correlated to the tumor's area. The temperature decreases as the area increases. In order to further investigate this relationship, the average and maximal temperature differences were plotted as a function of tumor area. The results are shown in Figs. 9 and 10, respectively.

It is evident that the slope of the fitted trend lines does not change if there is a constant error or offset in the measurement or estimation of the area or temperatures (and, therefore, it hardly changes if the caliper measurements are used instead of the estimation). Instead, the plotted points and trend line are moved up or down (in case of temperature constant offset) or left and right (constant area offset).

A few noteworthy conclusions can be derived from these graphs. The general behavior of the temperature difference (either average or maximal) as a function of the area seemed

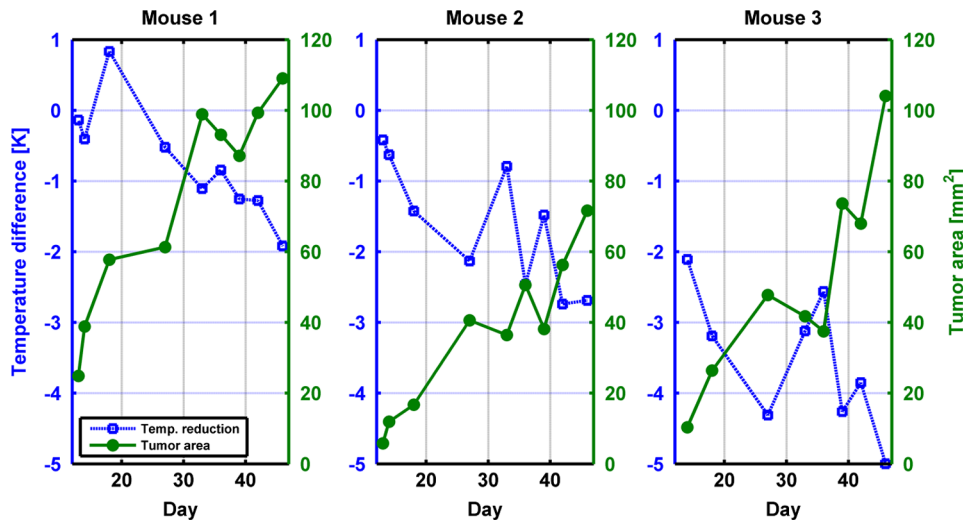


Fig. 7 Tumor area (circular markers, scale on the right) and average temperature difference (square markers, scale on the left) as a function of time.

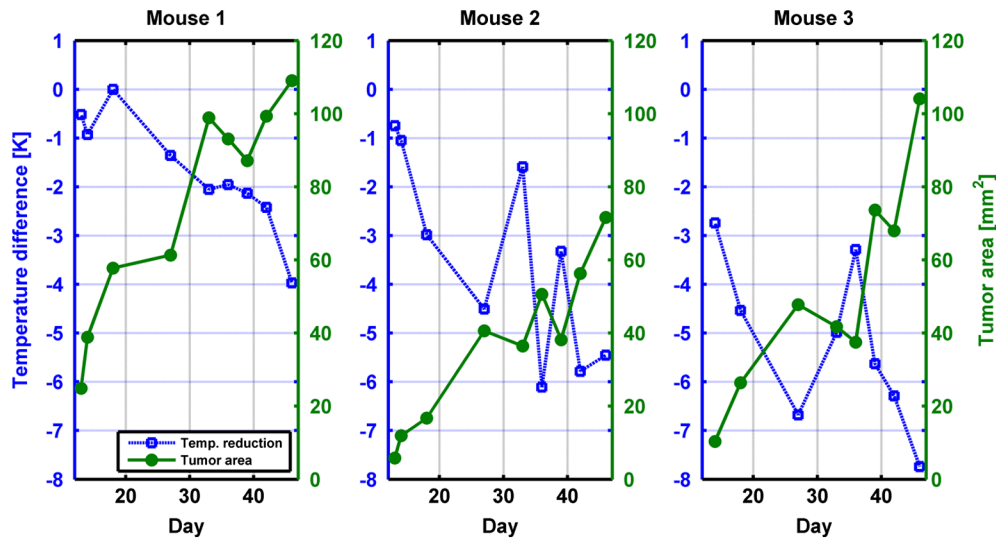


Fig. 8 Tumor area (circular markers, scale on the right) and maximal temperature difference (square markers, scale on the left) as a function of time.

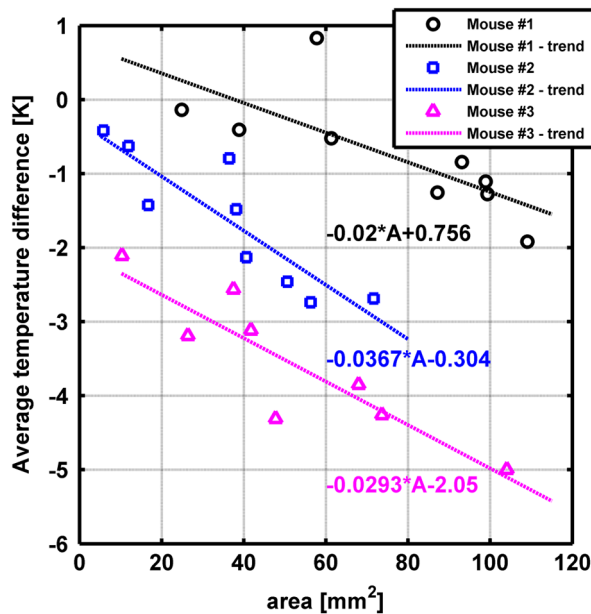


Fig. 9 Average temperature difference as a function of estimated tumor area. A linear fit for each mouse appears as a line along with its equation.

to be the same. The tumor temperature decreases as its area increases. This can be explained by the necrosis at the center of the tumor and its extruding shape, typical to this type of transplantable tumors.

It was also cautiously observed (due to the small number of mice for this part) that the slopes for all mice are similar. For example, a growth of 10 mm² in tumor area seemed to be linked to a reduction of 0.2 to 0.36 deg in the average tumor temperature, indicating that the biological and physical characteristics of the tumor (such as the necrotic center and a similar growth pattern) created similar heat transfer patterns for varying areas.

The small changes between line slopes in the graphs were hypothesized to be indicative of internal biological changes. For example, the larger slope of mouse #2 graph could indicate

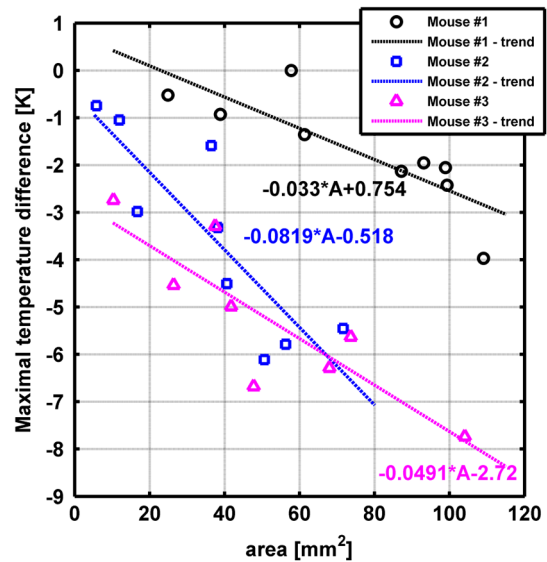


Fig. 10 Maximal temperature difference as a function of estimated tumor area. A linear fit for each mouse appears as a line along with its equation.

a stronger reduction in tumor temperature, which may be attributed to lower metabolic and perfusion rates in the tumor due to the treatment. One should have expected to see this result in mouse #1, but the collapse of the necrotic shell prevented reaching any significant conclusions.

In order to test these hypotheses, a second experiment was conducted including nine mice, six of which were injected with DaRT wires and three with inert wires. These mice were imaged four times in order to calculate the slopes described before. In this experiment, the tumors were smaller and the treatment had begun at an earlier stage.

Figure 11 shows visual and thermal images of one of the inert treated mice's tumor at days 15 and 29 of the experiment, while its area was 15.5 and 50.4 mm², respectively. As the figure shows, unlike in the first experiment, tumors were not always

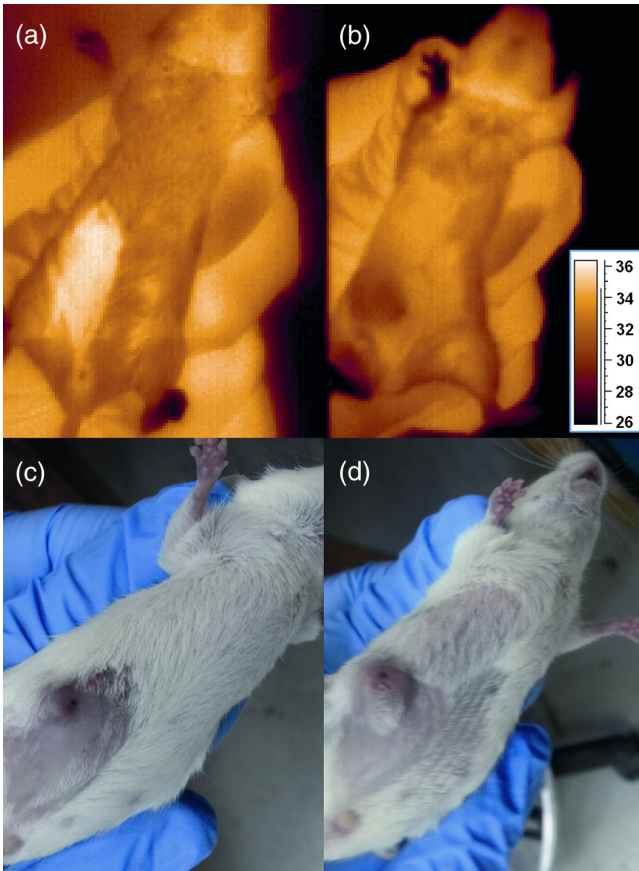


Fig. 11 Visual and thermal images of an inert-treated mouse at days 15 and 29 of the second experiment. (a) Thermal image at day 15. (b) Thermal image at day 29. (c) Visual image at day 15. (d) Visual image at day 29. The temperature scale appearing in (b) is relevant for (a) as well.

easy to detect in the thermal images at the initial stages of their growth (probably due to their small size). Although the temperature pattern caused by the tumor was similar to the pattern shown in the first experiment (cooler elliptical area), the temperature differences compared to the skin were smaller and the tumor was sometimes partially obscured by other features in the image.

The procedure in this experiment was similar to the one described for the thermal images in the first experiment and is illustrated in Fig. 12. The image was rotated if necessary, scaled and cut to a smaller image around the tumor. In order to locate the tumor and its boundaries in the most accurate manner possible, the visual images were used to help find the tumor in the thermal images. The tumor was then manually marked on the thermal image and its calculated area was compared to the caliper measurements. If the estimated tumor was too small or large, the process was repeated until an area difference of 20% or less was achieved. The hottest point at each image, indicating shaved abdomen skin tissue, was selected as the reference healthy skin tissue temperature and was subtracted from the entire image. The estimated tumor boundaries were used to calculate the tumor's maximal and average temperature differences compared to the reference temperature.

Figure 13 presents the caliper-measured average area of the tumors for all the mice measured during the entire second experiment (i.e., excluding two mice).

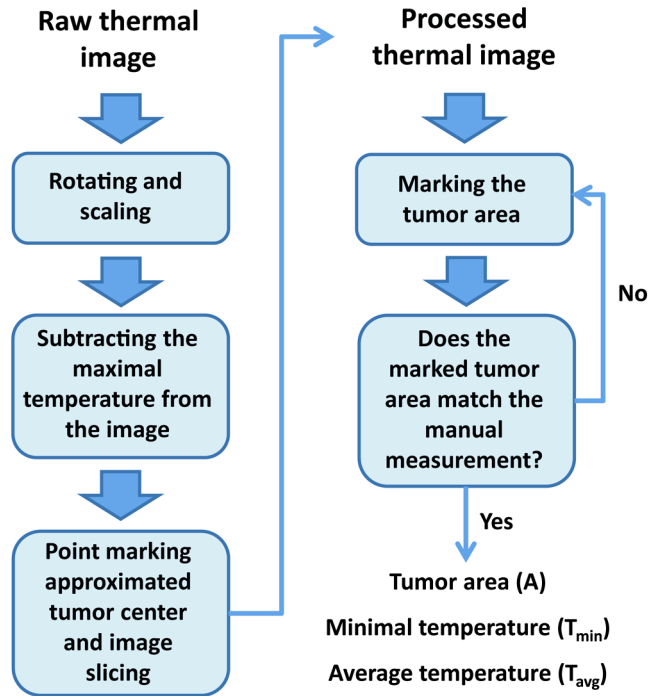


Fig. 12 Analysis procedure for the second mice experiment.

DaRT treatment increased their tumor area by 78% in comparison to mice with inert wires, which increased their tumor area by 165%.

The average and maximal temperature differences between the tumor and the healthy skin tissue temperature were calculated and presented in Figs. 14 and 15, respectively. Since the average temperature greatly depends on the area of the estimated tumor, and due to the small areas of the tumors, the estimated tumor areas were used to calculate the average temperature differences. Therefore, errors caused by different tumor area estimations were reduced.

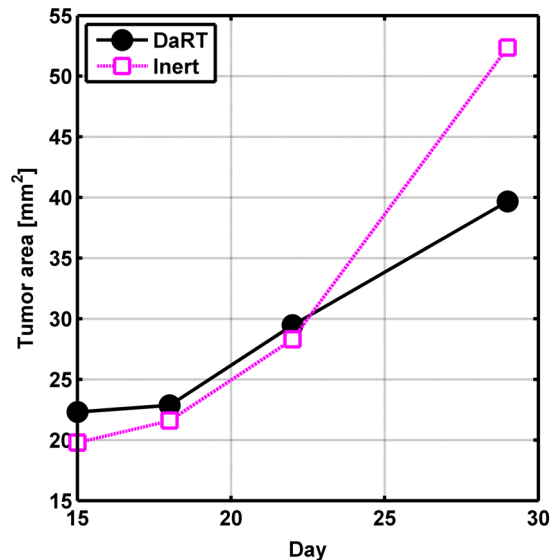


Fig. 13 Caliper-measured average area of the tumors for all the mice participating during the entire experiment (i.e., excluding two mice that died in the middle of the experiment). On average, mice with DaRT treatment increased their tumor area by 78% in comparison to mice with inert wires, which increased their tumor area by 165%.

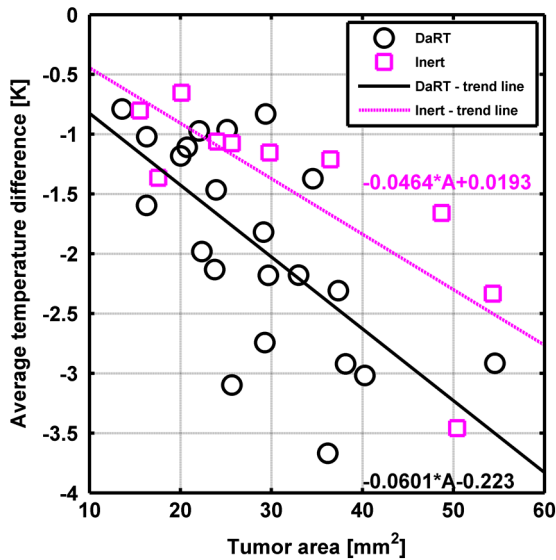


Fig. 14 Average temperature difference as a function of estimated tumor area. A linear fit for each group appears as a line along with its equation.

As the figures show, all tumors exhibited a pattern similar to the one observed in the first experiment: the tumors were colder than their surroundings and their temperature further reduced as their area increased. The calculated slopes for the DaRT-treated tumors were larger than the slopes calculated for the tumors with inert wires. Both slopes were relatively similar to each other and were only slightly higher than the slopes calculated in the first experiment.

Since the tumor temperature differences exhibit a linear dependence on the area ($\Delta T = a \cdot A + b$, where ΔT is the average or maximal temperature difference and A is the tumor area), it is expected that, on average, the ratio between the temperature difference change and the area change between measurements

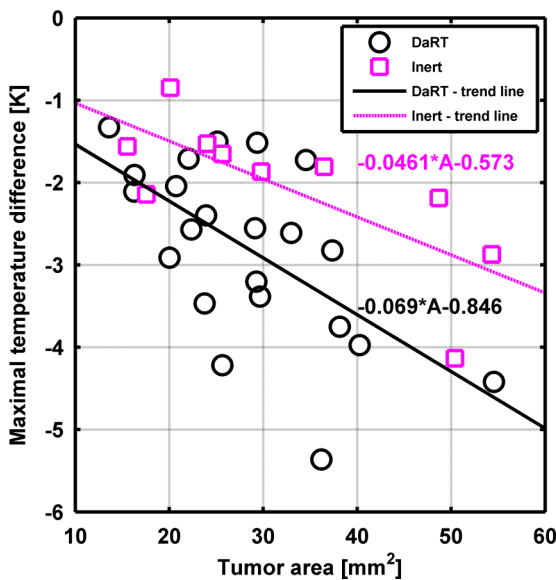


Fig. 15 Maximal temperature difference as a function of estimated tumor area. A linear fit for each group appears as a line along with its equation.

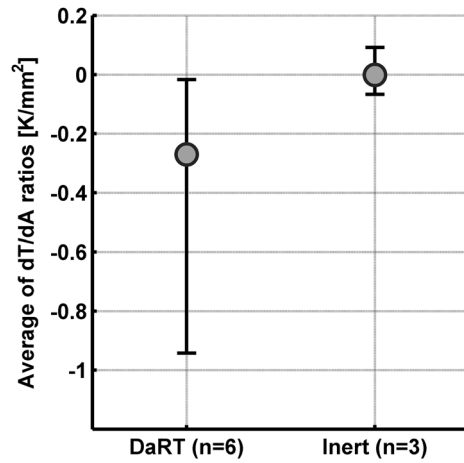


Fig. 16 Ratio of (changes in average tumor temperature difference) to (changes in tumor area), averaged on all mice during the second experiment.

will be similar to the slopes calculated, as demonstrated by Eq. (3):

$$\frac{\Delta T_n - \Delta T_m}{A_n - A_m} = \frac{(a \cdot A_n + b) - (a \cdot A_m + b)}{A_n - A_m} = a, \quad (3)$$

where the indices n and m indicate the corresponding values for days n and m , respectively.

For each mouse, the ratio described in Eq. (3) was calculated between all consecutive measurements (a total of three ratios for each mouse, excluding the two mice that had only two measurements and therefore only one ratio could be calculated).

Figures 16 and 17 show the calculated ratios for the DaRT and inert wire treatment groups, between the average (in Fig. 16) and maximal (in Fig. 17) temperature difference changes and the area changes, averaged for each group. The error bars represent the range of all averages.

As shown in the figures, DaRT-treated tumors have a larger ratio on average $[-0.27$ and -0.313 (K/mm^2) for the average and maximal temperature differences, respectively] than the inert-treated tumors $[-5 \times 10^{-4}$ and 0.0335 (K/mm^2)]. These values mean that the temperature of DaRT-treated tumors

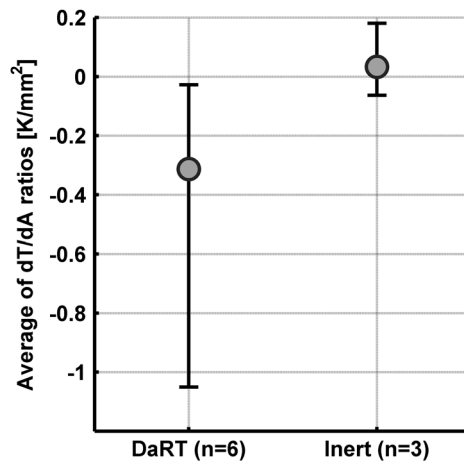


Fig. 17 Ratio of (changes in maximal tumor temperature difference) to (changes in tumor area), averaged on all mice during the second experiment.

decreases at an increased rate when compared to tumors with inert wires. This finding possibly indicates reduced metabolic activity due to the destruction processes caused by the treatment, leading to reduced heat production. Both ratio groups seem to be almost separated and distinct, although they have a small overlap. It is also interesting to observe the differences between mice in the DaRT treatment group. On average, both mice with the inhibited immune system had a ratio of -0.132 (K/mm²), while the other mice on this group had a calculated ratio of -0.34 (K/mm²) (for the average temperature difference). This finding (although calculated for a small sample size) may suggest that a different biological process occurs for these mice.

Unlike in the first experiment, no breakdown of the necrotic shell above tumors was observed in the second experiment. Therefore, the same thermal patterns were maintained for the DaRT-treated tumor group, simplifying the analysis and improving the validity of the results.

In order to compare these findings with previous experimental results found by other research groups, tumor sizes, temperature differences, and their correlation were extracted from graphs in papers describing the progress of human MDA-MB-231, MCF7, and rat 13762 MAT tumors^{23,24} in mice. The slopes were calculated from the first day the tumors were detected and were found as -0.0359 , -0.1369 , and -0.011 (K/mm²), respectively. The relatively low slope for the 13762 MAT tumors may be explained by the fact that this type of tumor is originated from rat tumor cells. Therefore they are more adapted to growth in mice tissues, leading to higher viability of the tumor and reduced necrosis and lower temperature differences.

4 Discussion and Conclusions

Thermal images showing the development of DA3 tumors in mice before and after treatment were presented. Tumor area was estimated for the larger tumors and comparability with manual measurements was shown. The correlation between estimated tumor area and temperature difference between the tumor and its surroundings was also calculated and presented. Overall, all mice depicted a similar behavior for this correlation. More specifically, treated mice were expected to show higher slopes, as treatment should induce more necrosis and therefore larger thermal differences. In the first experiment, this was seen when treated mouse #2 was compared to untreated mouse #3. However, it was not seen when treated mouse #1 was compared to treated mouse #3. This can be explained by the different morphology of the tumor of mouse #1. This effect was observed more clearly in the second experiment.

In both experiments, area estimation was based on visual examination of the image and manually defining tumor borders. For the second experiment, this process is illustrated in Fig. 12. The complex surroundings of the tumors, especially when dealing with small tumors (smaller than ~ 30 mm²), have made the detection and area estimation difficult (as seen in Fig. 11), making automated and semi-automated algorithms inaccurate in this case. This topic should definitely be improved in future research.

Tumor identification could benefit from improved integration of the visual and thermal images. A possible method to perform such integration is by placing markers near the tumor and using them to locate it and cross-correlate between the images, as implemented in other works.¹⁶

Repeating the experiment with a larger sample size revealed that the slope difference between the treated and inert wire groups was actually larger than expected from the first experiment and that the slope obtained for mouse #2 was small relative to the average slope for this group.

Two steps should be considered in order to further strengthen the validity of the results. The first step is to increase the sample size of mice and measurements in order to establish more rigid statistics, expanded to additional tumor types, treatments, and sizes. The second step is to explain the high temperature difference between tumors and their surroundings. This difference is up to 8°C and is higher than was expected. It can be explained by either a different emissivity of the tumor or by heat loss due to the lack of blood perfusion and low thermal conductivity at the tumor surface.

The correlation between temperature differences and tumor area can be used to further improve tumor area estimation by cross-checking area estimations in comparison to the estimated average temperature and the tumor's temperature change to area change specific ratio. In addition, since measuring the maximal temperature difference does not require accurate detection of tumor boundaries, it may be extremely useful to find the relevant gradient for the inspected mouse at the initial days of the experiment and use it to perform quick size estimation at later stages using a simple process—estimation of the healthy tissue temperature and locating the coldest spot in the tumor.

Future work should expand this method to other types of tumors as it could reveal a significantly unique temperature difference/area relation for each tumor type. This could provide a future tool for the indication of abnormal behaviors during tumor development. Future work should also consider the use of simulations (e.g., finite elements method simulations) and experiments in phantoms. By doing so, the effect of physical parameters, such as size and shape, can be isolated from effects resulted solely from biological changes.

In conclusion, the correlation between tumor temperature and area was investigated, presenting a potentially useful tool for tumor development assessment. Unlike common methods such as tumor size measurement by a caliper, this method has the advantage of not only being noninvasive but being non-contact as well. In addition, this method is nonradiative and low cost, which provides a significant advantage over methods such as CT and PET-CT. Last, thermal images provide indication of biological processes (e.g., necrosis) that are important when tumor development is being monitored and are difficult to acquire by other methods.

References

1. P. Therasse et al., "New guidelines to evaluate the response to treatment in solid tumors," *J. Natl. Cancer Inst.* **92**(3), 205–216 (2000).
2. M. M. Tomayko and C. P. Reynolds, "Determination of subcutaneous tumor size in athymic (nude) mice," *Cancer Chemother. Pharmacol.* **24**(3), 148–154 (1989).
3. D. M. Euhus et al., "Tumor measurement in the nude mouse," *J. Surg. Oncol.* **31**(4), 229–234 (1986).
4. M. Diakides, J. D. Bronzino, and D. R. Peterson, *Medical Infrared Imaging—Principles and Practices*, CRC Press, Boca Raton, FL (2013).
5. S. Bagavathiappan et al., "Infrared thermal imaging for detection of peripheral vascular disorders," *J. Med. Phys.* **34**(1), 43–47 (2009).
6. M. Banić et al., "Thermography in patients with inflammatory bowel disease and colorectal cancer: evidence and review of the method," *Periodicum Biologorum* **113**(4), 439–444 (2011).

7. T. J. Love, "Thermography as an indicator of blood perfusion," *Ann. N. Y. Acad. Sci.* **335**(1), 429–437 (1980).
8. P. Bacon et al., "Thermography in the assessment of inflammatory arthritis," in *Clinics in Rheumatic Diseases. Diagnosis and Management*, M. Jayson, Ed., pp. 21: 51–66, WB Saunders, London (1976).
9. W. C. Amalu et al., "Infrared imaging of the breast—An overview," Chapter 25 in *The Biomedical Engineering Handbook. Medical Devices and Systems*, J. D. Bronzino, Ed., pp. 25-1–25-21, CRC Press, Boca Raton, FL (2006).
10. M. Gautherie and C. M. Gros, "Breast thermography and cancer risk prediction," *Cancer* **45**(1), 51–56 (1980).
11. M. Gautherie, "Thermobiological assessment of benign and malignant breast diseases," *Am. J. Obstet. Gynecol.* **8**(147), 861–869 (1983).
12. M. Gautherie, A. Kotewicz, and P. Gueblez, "Accurate and objective evaluation of breast thermograms: basic principles and new advances with special reference to an improved computer-assisted scoring system," in *Thermal assessment of breast health: proceedings of an international conference*, Washington, DC, pp. 72–97, MTP Press Ltd (1984).
13. S. Fok, E. Y. K. Ng, and K. Tai, "Early detection and visualization of breast tumor with thermogram and neural network," *J. Mech. Med. Biol.* **2**(02), 185–195 (2002).
14. M. Mital and E. P. Scott, "Thermal detection of embedded tumors using infrared imaging," *J. Biomech. Eng.* **129**(1), 33–39 (2007).
15. J. P. Agnelli, A. Barrea, and C. Turner, "Tumor location and parameter estimation by thermography," *Math. Comput. Model.* **53**(7), 1527–1534 (2011).
16. A. L. Shada et al., "Infrared thermography of cutaneous melanoma metastases," *J. Surg. Res.* **182**(1), e9–e14 (2013).
17. P. Vaupel, F. Kallinowski, and P. Okunieff, "Blood flow, oxygen and nutrient supply, and metabolic microenvironment of human tumors: a review," *Cancer Res.* **49**(23), 6449–6465 (1989).
18. R. A. Macbeth and J. G. Bekesi, "Oxygen consumption and anaerobic glycolysis of human malignant and normal tissue," *Cancer Res.* **22**(2), 244–248 (1962).
19. F. Kallinowski et al., "Blood flow, metabolism, cellular microenvironment, and growth rate of human tumor xenografts," *Cancer Res.* **49**(14), 3759–3764 (1989).
20. T. Yahara et al., "Relationship between microvessel density and thermographic hot areas in breast cancer," *Surg. Today* **33**(4), 243–248 (2003).
21. J. M. Luna et al., "Procedure to estimate thermophysical and geometrical parameters of embedded cancerous lesions using thermography," *J. Biomech. Eng.* **134**(3), 031008 (2012).
22. V. Umadevi, S. Raghavan, and S. Jaipurkar, "Framework for estimating tumour parameters using thermal imaging," *Indian J. Med. Res.* **134**(5), 725–731 (2011).
23. W. Xie et al., "Evaluation of the ability of digital infrared imaging to detect vascular changes in experimental animal tumours," *Int. J. Cancer* **108**(5), 790–794 (2004).
24. C. Song et al., "Thermographic assessment of tumor growth in mouse xenografts," *Int. J. Cancer* **121**(5), 1055–1058 (2007).
25. S. A. Kirubha et al., "Evaluation of mammary cancer in 7, 12-Dimethylbenz (a) anthracene-induced Wistar rats by asymmetrical temperature distribution analysis using thermography: a comparison with serum CEA levels and histopathology," *BioMed Res. Int.* **2012**, 786417 (2012).
26. L. Arazi et al., "Treatment of solid tumors by interstitial release of recoiling short-lived alpha emitters," *Phys. Med. Biol.* **52**(16), 5025–5042 (2007).
27. T. Cooks et al., "Growth retardation and destruction of experimental squamous cell carcinoma by interstitial radioactive wires releasing diffusing alpha-emitting atoms," *Int. J. Cancer* **122**(7), 1657–1664 (2008).
28. E. Lazarov et al., "Comparative in vitro microdosimetric study of murine-and human-derived cancer cells exposed to alpha particles," *Radiat. Res.* **177**(3), 280–287 (2012).
29. L. Arazi et al., "The treatment of solid tumors by alpha emitters released from ²²⁴Ra-loaded sources—internal dosimetry analysis," *Phys. Med. Biol.* **55**(4), 1203–1218 (2010).